Effect of Chemical Extraction of Lithium on the Local Structure of Spinel Lithium Manganese Oxides Determined by X-ray Absorption Spectroscopy

Brett Ammundsen,† Deborah J. Jones, and Jacques Rozière*

Laboratoire des Agrégats Moléculaires et Matériaux Inorganiques, ESA 5072 CNRS, Université Montpellier 2, Place Eugène Bataillon, 34095 Montpellier Cédex 5, France

Gary R. Burns*

Department of Chemistry, Victoria University of Wellington, P.O. Box 600, Wellington, New Zealand

Received May 20, 1996. Revised Manuscript Received July 17, 1996[⊗]

The local structural modifications resulting from chemical extraction and reinsertion of lithium in spinels of composition $LiMn_2O_4$ and $Li_{4/3}Mn_{5/3}O_4$ have been investigated by X-ray absorption spectroscopy (XAS) at the manganese K-edge. For $LiMn_2O_4$, Mn−O and Mn−Mn distances determined from the extended X-ray absorption fine structure (EXAFS) decrease significantly when lithium is extracted in 0.1 M HCl, but are restored to their original values when ∼90% of the lithium content is reconstituted by sorption in LiOH solution. The Mn−O and Mn−Mn distances for $Li_{4/3}Mn_{5/3}O_4$ are shorter than for $LiMn_2O_4$, consistent with a higher manganese oxidation state and lower unit cell parameter for this compound, and show much smaller variations on lithium extraction and reinsertion. In addition lithium extraction from $LiMn_2O_4$ results in an increase in local structural order, followed by a return to the lower symmetry state of the parent material when lithium is reinserted. These changes are not observed in the spectra of $Li_{4/3}Mn_{5/3}O_4$ and its delithiated or relithiated products, which show rather the effects of local structural perturbations due to manganese vacancies in octahedral sites. Evolution of the X-ray absorption near-edge structure (XANES), in particular the position of the main edge discontinuity and modifications in the pre-edge spectral structure, supports chemical analyses in showing that lithium extraction from $LiMn_2O_4$ produces a Mn^{IV}-type spinel oxide from a mixed Mn^{III}/Mn^{IV} parent material and that reinsertion of lithium results in a return to a mixed oxidation state. By contrast, the XANES data for $Li_{4/3}Mn_{5/3}O_4$ show that here the dominant manganese state is Mn^{IV} and that lithium extraction and reinsertion entail only trivial local electronic changes. The XAS results are therefore compatible with a mainly redox mechanism for lithium extraction and reinsertion for $LiMn_2O_4$, but a predominantly ion-exchange process in the case of $Li_{4/3}Mn_{5/3}O_4$, with the insertion of charge-compensating protons into the lattice.

Introduction

The chemical extraction of lithium from spinel phases of lithium manganese oxide gives materials which retain the spinel framework of the parent compounds and which are highly selective as sorbents for lithium in aqueous environments.[1−17] The reversibility of the sorption process is also exploited in nonaqueous rechargeable batteries where spinel manganese oxides serve as the cathode material.[18−31]

The mechanisms involved in the chemical extraction and insertion of lithium have been the subject of

† On leave from the Department of Chemistry, Victoria University of Wellington.

⊗ Abstract published in *Advance ACS Abstracts*, September 1, 1996.

(1) Hunter, J. C. *J. Solid State Chem.* **1981**, *39*, 142.
(2) Shen, X.-M.; Clearfield, A. J. *J. Solid State Chem.* **1986**, *64*, 270.
(3) Vol'khin, V. V.; Leont'eva, G. V.; Onolin, S. A. *Neorg. Mater.* **1973**, *6*, 1041.
(4) Leont'eva, G. V.; Chirkova, L. G. *Zh. Prikl. Khim.* **1988**, *61*, 734.
(5) Ooi, K.; Miyai, Y.; Katoh, S. *Sep. Sci. Technol.* **1986**, *21*, 755.
(6) Ooi, K.; Miyai, Y.; Katoh, S. *Sep. Sci. Technol.* **1987**, *22*, 1779.
(7) Ooi, K.; Miyai, Y.; Katoh, S.; Maeda, H.; Abe, M. *Langmuir* **1989**, *5*, 150.
(8) Ooi, K.; Miyai, Y.; Katoh, S.; Maeda, H.; Abe, M. *Langmuir* **1990**, *6*, 289.
(9) Ooi, K.; Miyai, Y.; Sakakihara, J. *Langmuir* **1991**, *7*, 1167.
(10) Kanoh, H.; Ooi, K.; Miyai, Y.; Katoh, S. *Langmuir* **1991**, *7*, 1841.
(11) Burns, G. R.; Kane, C.; Sahasrabudhe, N. In *New Developments in Ion Exchange*; Abe, M., Kataoka, T., Suzuki, T., Eds.; Kodansha and Elsevier: Tokyo, Amsterdam, 1991; p 523.
(12) Feng, Q.; Miyai, Y.; Kanoh, H.; Ooi, K. *Langmuir* **1992**, *8*, 1861.
(13) Kanoh, H.; Ooi, K.; Miyai, Y.; Katoh, S. *Sep. Sci. Technol.* **1993**, *28*, 643.
(14) Kanoh, H.; Feng, Q.; Miyai, Y.; Ooi, K. *J. Electrochem. Soc.* **1993**, *140*, 3162.
(15) Kanoh, H.; Feng, Q.; Miyai, Y.; Ooi, K. *J. Electrochem. Soc.* **1995**, *142*, 702.
(16) Feng, Q.; Kanoh, H.; Miyai, Y.; Ooi, K. *Chem. Mater.* **1995**, *7*, 1226.
(17) Ammundsen, B.; Jones, D. J.; Rozière, J.; Burns, G. R. *Chem. Mater.* **1995**, *7*, 2151.
(18) Pistoia, G. *J. Electrochem. Soc.* **1982**, *129*, 1861.
(19) Thackeray, M. M.; David, W. I. F.; Bruce, P. G.; Goodenough, J. B. *Mater. Res. Bull.* **1983**, *18*, 461.
(20) Thackeray, M. M.; Johnson, P. J.; de Picciotto, L. A.; Bruce, P. G.; Goodenough, J. B. *Mater. Res. Bull.* **1984**, *19*, 179.
(21) Ohzuku, T.; Kitagawa, M.; Hirai, T. *J. Electrochem. Soc.* **1990**, *137*, 769.
(22) Tarascon, J. M.; Wang, E.; Shokoohi, F. K.; McKinnon, W. R.; Colson, S., *J. Electrochem. Soc.* **1991**, *138*, 2859.
(23) Guyomard, D.; Tarascon, J. M. *J. Electrochem. Soc.* **1992**, *139*, 937.
(24) Rossouw, M. H.; de Kock, A.; de Picciotto, L. A.; Thackeray, M. M.; David, W. I. F.; Ibberson, R. M. *Mater. Res. Bull.* **1990**, *25*, 173.

S0897-4756(96)00287-6 CCC: $12.00

discussion since the extraction process in acid solution was first reported for $LiMn_2O_4$ by Hunter.[1] A redox mechanism was proposed for the extraction, involving disproportionation of lattice Mn^{III} to give a manganese(IV) oxide phase "λ-MnO_2" and dissolved Mn^{2+}. In solutions containing dissolved lithium at pH above 4, the λ-MnO_2 material sorbs lithium ions by reinsertion into the spinel lattice, a reaction which appears to proceed with reduction of an equivalent of lattice Mn^{IV} to Mn^{III}.[7−9,12] At least in the case of $LiMn_2O_4$ prepared at temperatures of 700−850 °C, a predominantly redox mechanism seems to be supported by experimental data which show up to 25% dissolution of the lithium manganate accompanied by formation of solution Mn^{2+} during lithium extraction, and evolution of oxygen during lithium reinsertion. The presence of a small amount of permanganate in solution after lithium extraction has also been observed but has been attributed to a "side" reaction.[32]

For lithium manganates prepared at lower temperatures, different behavior has been observed.[2,9,12] When lithium is extracted from such materials in acid solution, charge compensation is achieved by insertion of protons. The ion exchange behavior appears to be related to higher Mn^{IV} content in these compounds.[9,12,17] Between 300 and 700 °C a range of stoichiometric lithium manganese oxide spinels can be prepared having the general formula $Li[Li_xMn_{2-x}]O_4$ where $0 \le x \le 0.33$, as well as apparently nonstoichiometric "oxygen-rich" spinels containing cation vacancies.[9,12,17,24−27,33−35] In the stoichiometric $Li[Li_xMn_{2-x}]O_4$ series the end members are $LiMn_2O_4$ ($x = 0$) and $Li_{4/3}Mn_{5/3}O_4$ ($x = 0.33$). The Mn^{III}/Mn^{IV} ratios in these compounds are theoretically equal to 1 and 0, respectively; therefore while $LiMn_2O_4$ might be expected to present redox behavior, lithium extraction from $Li_{4/3}Mn_{5/3}O_4$ should occur mainly by exchange with protons. However, it has recently been pointed out that an overall manganese oxidation state of 4 is practically never attained, as shown by chemical analyses of "$Li_{4/3}Mn_{5/3}O_4$" preparations.[33] In addition, the reversibility of the ion-exchange mechanism has been questioned since a maximum of only 60−70% reinsertion of the original lithium content is observed for the protonated materials,[12,17] compared with greater than 90% in the case of those materials for which a redox process is expected to predominate.

The purpose of the study presented here was to provide additional data on these systems by applying X-ray absorption spectroscopy (XAS) and thereby compare the chemical and structural changes accompanying lithium extraction and reinsertion in spinels of composition $LiMn_2O_4$ and $Li_{4/3}Mn_{5/3}O_4$. XAS probes the local electronic and geometric structure around a selected absorbing atom, in this study manganese. Structural information such as interatomic distances and coordination numbers can be determined for nearby coordination shells from the extended X-ray absorption fine structure (EXAFS), and semiquantitative information concerning valency and bonding can be derived from X-ray absorption near-edge structure (XANES).[36] In the case of manganese compounds, chemical effects in the K-edge XANES such as the position of the absorption jump and the structure of pre-edge features have been shown to be sensitive to the effective charge on the absorbing manganese ion and therefore correlated with manganese oxidation state.[37−42] In this paper we compare information obtained from X-ray absorption spectroscopy with the results of chemical analyses and determination of the bulk average crystal structure using powder X-ray diffraction.

Experimental Section

Samples. $LiMn_2O_4$ was prepared by firing a finely ground mixture of lithium and manganese carbonate in molar ratio 0.5 at 800 °C in air for 24 h. To prepare the sample of $Li_{4/3}Mn_{5/3}O_4$, a carbonate mixture with Li/Mn molar ratio 0.8 was fired at 400 °C in air for 8 h. Lithium was extracted from these compounds to give "λ-MnO_2" products by stirring in 0.2 M HCl for 72 h, after which the samples were washed thoroughly with distilled water and dried at 60 °C. Reinsertion of lithium in the "λ-MnO_2" samples was achieved by stirring in 0.1 M LiOH for 120 h. β-MnO_2 (Aldrich product of 99.5% purity) and α-Mn_2O_3 (prepared by decomposition of β-MnO_2 in air at 770 °C) were selected as reference compounds for octahedrally coordinated Mn^{IV} and Mn^{III} respectively.

X-ray Diffraction and Chemical Analyses. Powder X-ray diffraction (XRD) with Cu Kα radiation using an automated Phillips diffractometer provided evidence for only one crystalline spinel phase for both lithium manganate preparations and their delithiated and relithiated products. Unit-cell parameters were calculated from the powder patterns. The chemical composition of each sample was determined by analyzing for lithium and manganese content by atomic emission spectrometry after dissolution in hydrochloric acid and hydrogen peroxide. The available oxygen of all samples was determined by the sodium oxalate method,[43] from which the mean oxidation state of manganese was evaluated.

X-ray Absorption Measurements. X-ray absorption spectra were recorded in transmission mode on the EXAFS 3 spectrometer at the French synchrotron facility DCI at LURE, using a Si [311] double monochromator slightly detuned for harmonic rejection. XANES spectra were recorded from ca. 100 eV before the Mn K-edge (6539 eV) to 100 eV after the

(25) de Kock, A.; Rossouw, M. H.; de Picciotto, L. A.; Thackeray, M. M.; David, W. I. F.; Ibberson, R. M. *Mater. Res. Bull.* **1990**, *25*, 657.
(26) Thackeray, M. M.; de Kock, A.; Rossouw, M. H.; Liles, D. C.; Bittihn, R.; Hoge, D. *J. Electrochem. Soc.* **1992**, *139*, 363.
(27) Thackeray, M. M.; de Kock, A.; David, W. I. F. *Mater. Res. Bull.* **1993**, *28*, 1041.
(28) Gummow, R. J.; de Kock, A.; Thackeray, M. M. *Solid State Ionics* **1994**, *69*, 59.
(29) Thackeray, M. M. *J. Electrochem. Soc.* **1995**, *142*, 2558.
(30) Richard, M. N.; Fuller, E. W.; Dahn, J. R. *Solid State Ionics* **1994**, *73*, 81.
(31) Barker, J.; West, K.; Saidi, Y.; Pynenburg, R.; Zachau-Christiansen, B.; Koksbang, R. *J. Power Sources* **1995**, *54*, 475.
(32) Kanzaki, Y.; Taniguchi, A.; Abe, M. *J. Electrochem. Soc.* **1991**, *138*, 333.
(33) Le Cras, F.; Strobel, P.; Anne, M.; Bloch, D.; Soupart, J.-P.; Rousche, J.-C. *Eur. J. Solid State Inorg. Chem.* **1996**, *33*, 67.
(34) Takada, T.; Hayakawa, H.; Akiba, E. *J. Solid State Chem.* **1995**, *115*, 420.
(35) Takada, T.; Hayakawa, H.; Kumagai, T.; Akiba, E. *J. Solid State Chem.* **1996**, *121*, 79.
(36) *X-ray Absorption: Principles, Applications, Techniques of EXAFS, SEXAFS, and XANES*; Koningsberger, D. C., Prins, R., Eds.; Wiley: New York, 1988.
(37) Salem, S. I.; Chang, C. N.; Lee, P. L.; Severson, V. *J. Phys. C: Solid State Phys.* **1978**, *11*, 4085.
(38) Sarode, P. R.; Ramasesha, S.; Madhusudan, W. H.; Rao, C. N. R. *J. Phys. C: Solid State Phys.* **1979**, *12*, 2439.
(39) Belli, M.; Bianconi, A.; Burattini, E., Mobilio, S.; Palladino, L., Reale, A.; Scafati, A. *Solid State Commun.* **1980**, *35*, 355.
(40) Apte, M. Y.; Mande, C. *J. Phys. C: Solid State Phys.* **1982**, *15*, 607.
(41) Lenglet, M.; Lopitaux, J.; Guillamet, R. *Mater. Chem. Phys.* **1986**, *14*, 199.
(42) Manceau, A.; Gorshkov, A. I.; Drits, V. A. *Am. Miner.* **1992**, *77*, 1133.
(43) Katz, M. J.; Clarke, R. C.; Nye, W. F. *Anal. Chem.* **1956**, *28*, 507.

edge in a 0.3 eV step size, and EXAFS spectra in a 1.5 eV step size to 900 eV after the absorption edge. He/Ne-filled ionization chambers were used to measure the incident and transmitted X-ray flux. Calibration was carried out prior to all measurements using a 10 μm Mn-foil by assigning E_0 to the first point of inflection in the absorption edge. Spectra were recorded on samples diluted in boron nitride powder at proportions calculated to give an edge jump in $\log(I_0/I)$ of ca. 1. Nujol mulls were pressed between the Parafilm windows of stainless-steel holders and maintained at 77 K in a cold-finger cryostat.

EXAFS and XANES Data Analyses. Experimental data were analyzed using the XAS programmes of Michalowicz.[44] XANES spectra were normalized to an edge jump of unity after removal of the background absorption by subtraction of a linear function extrapolated from the pre-edge. EXAFS spectra were normalized in the $\mu_{1,\mathrm{exp}} - \mu_{0,\mathrm{exp}}$ convention after simulating the atomic absorption $\mu_{0,\mathrm{exp}}$ with third-order polynomials or spline functions. Fourier transformations using a Kaiser apodization window ($\tau = 3.5$) were performed over the k range 2.5−14 Å^{-1} using k^3 weighting to compensate for attenuation of the amplitude in the EXAFS spectra at high k.

Quantitative analyses of EXAFS spectra to determine R_i, the distance of the ith shell of atoms from the absorbing manganese atom, and σ_i, the Debye−Waller factor, were performed for the spinel compounds using curve-fitting procedures in k space after Fourier filtering to isolate the EXAFS signal $\chi(k)$ corresponding to the relevant maxima in the Fourier transformations. Theoretical curves were simulated using functions for the backscattering amplitude $F_i(k)$ and total phase shift $\phi_i(k)$ calculated for the corresponding scattering paths by the tabulated values of McKale et al.[45] and by the ab initio XAS code FEFF6 developed by Rehr and co-workers.[46−49] FEFF's ab initio calculated function for the photoelectron mean free path $\lambda(k)$ was also used, so that the only independent parameters in the curve-fitting procedure other than R_i and σ_i were the coordination numbers N_i for each shell, the overall amplitude reduction factor S_0^2, and adjustments of the threshold energy origin E_0. The coordination number for the first shell of oxygen atoms was fixed to the crystallographic value of 6 for all the samples. In the case of the second coordination shell, consisting of manganese atoms in neighboring 16d octahedral sites, the coordination number was refined in the range 4−6. The amplitude reduction factor S_0^2 was scaled to 0.86 after a preliminary refinement for the λ-MnO_2 product of $LiMn_2O_4$, and only very small adjustments for the energy origin E_0 ($1 < \Delta E_0 < 4$) were required for each path to optimise the fits of the theoretical data to the experimental data. In all cases the agreement between experimental and theoretical curves over the k range 2.5−14 Å^{-1} gave statistical residues of less than 2% (residue $= \sum_k(k[\chi_{\mathrm{exp}}(k)] - k[\chi_{\mathrm{th}}(k)])^2k^3/\sum_k(k[\chi_{\mathrm{exp}}(k)]^2)k^3$).

Ab initio curved-wave multiple-scattering EXAFS $\chi(k)$ and XANES $\mu(E)$ spectra were computed by FEFF6 using the atomic coordinates of spinel lithium manganates.[27,50] Clusters of 8−9 Å radius, comprising up to 250 atoms in 24 coordination shells, were constructed for the calculations of atomic scattering potentials, to ensure consistency among simulations for all atoms involved in significant scattering paths even when the path calculations were restricted to a smaller cluster volume. The Hedin−Lundqvist self-energy was used for the photoelectron, introducing a 1.5 eV correction to the imaginary part to model the effects of experimental resolution. Paths of up to 18 Å in total length were considered for multiple scattering computations, and those paths contributing a mean-path amplitude greater than 2.5% of that of the first shell maximum, as estimated by FEFF's curved-wave calculation, were included in the final calculation of the spectra.

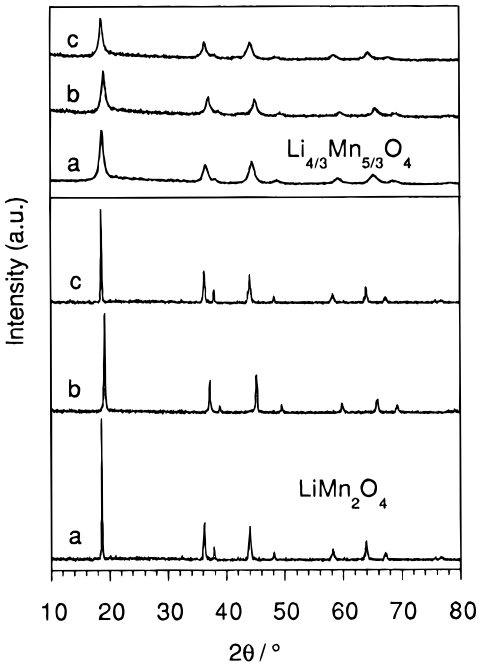

Figure 1. Powder X-ray diffraction patterns for $LiMn_2O_4$ and $Li_{4/3}Mn_{5/3}O_4$: (a) parent compounds, (b) lithium-extracted samples, and (c) lithium-reinserted samples.

Results and Discussion

Powder X-ray Diffraction and Chemical Analyses. Powder X-ray diffraction patterns for the $LiMn_2O_4$ and $Li_{4/3}Mn_{5/3}O_4$ compounds and their lithium-extracted and -reinserted products are given in Figure 1. The lower temperature and shorter heating period used to prepare $Li_{4/3}Mn_{5/3}O_4$ results in a sample of lower crystallinity than $LiMn_2O_4$, as indicated by the lower intensity and broader diffraction lines in the XRD patterns. Unit-cell parameters calculated from the powder patterns are given in Table 1. Chemical formulas for the samples were calculated from the analyses of lithium and manganese contents and manganese oxidation state. In the chemical formulation for the lithium-extracted and lithium-reinserted products of "$Li_{4/3}Mn_{5/3}O_4$" given in Table 1, hydrogen ions have been included consistent with charge neutrality and with experimental results discussed elsewhere.[17]

The lithium/manganese ratio and value for the bulk oxidation state of the parent $LiMn_2O_4$ compound agree with the ideal formula to within ±4%, and the unit-cell parameter is close to that previously reported for this composition crystallized at 700−850 °C.[27,51] For the $Li_{4/3}Mn_{5/3}O_4$ sample a value of 3.89 was obtained for the average manganese oxidation state. The Li/Mn ratio of 0.787 determined by chemical analysis would imply for a stoichiometric spinel a mean manganese oxidation state of 3.976. The difficulty of preparing stoichiometric "$Li_{4/3}Mn_{5/3}O_4$" (Li/Mn = 0.8) has recently been discussed,[33] and it has been proposed that a manganese oxidation state in the vicinity of 3.9 is an experimental limit for one-phase spinels having the highest Li/Mn

(44) Michalowicz, A. In *Logiciels pour la Chimie*; Société Française de Chimie: Paris, 1991; p 102.
(45) McKale, A. G.; Veal, B. W.; Paulikas, A. P., Chan, S.-K.; Knapp, G. S. *J. Am. Chem. Soc.* **1988**, *110*, 3763.
(46) Rehr, J. J.; Mustre de Leon, J.; Zabinsky, S. I.; Albers, R. C. *J. Am. Chem. Soc.* **1991**, *113*, 5135.
(47) Mustre de Leon, J.; Rehr, J. J.; Zabinsky, S. I.; Albers, R. C. *Phys. Rev. B* **1991**, *44*, 4146.
(48) Rehr, J. J.; Booth, C. H.; Bridges, F.; Zabinsky, S. I. *Phys. Rev. B* **1994**, *49*, 12347.
(49) Zabinsky, S. I.; Rehr, J. J.; Ankudinov, A.; Albers, R. C.; Eller, M. J. *Phys. Rev. B* **1995**, *52*, 2995.
(50) Fong, C.; Kennedy, B. J.; Elcombe, M. M. *Z. Kristallogr.* **1994**, *209*, 941.

Table 1. Compositional and Structural Parameters for the Spinel Compounds

sample	a_0 (Å)	Li/Mn ratio	mean oxidation state of Mn	chemical formula
"$LiMn_2O_4$"	8.24	0.480	3.48	$Li_{0.96}Mn^{III}_{1.04}Mn^{IV}_{0.98}O_4$
lithium-extracted	8.02	0.054	3.95	$Li_{0.11}Mn^{III}_{0.11}Mn^{IV}_{1.89}O_4$
lithium-reinserted	8.24	0.444	3.56	$Li_{0.89}Mn^{III}_{0.89}Mn^{IV}_{1.11}O_4$
"$Li_{4/3}Mn_{5/3}O_4$"	8.15	0.787	3.89	$Li_{1.34}Mn^{III}_{0.18}Mn^{IV}_{1.53}O_4$
lithium-extracted	8.04	0.015	3.97	$Li_{0.03}H_{1.18}Mn^{III}_{0.05}Mn^{IV}_{1.66}O_4$
lithium-reinserted	8.17	0.422	3.87	$Li_{0.73}H_{0.65}Mn^{III}_{0.22}Mn^{IV}_{1.49}O_4$

ratios. An oxidation state of 3.9 corresponds to a Li/Mn ratio ~0.75 if the spinel is assumed to be stoichiometric in oxygen. The slightly higher Li/Mn ratio of 0.787 found for our sample can be explained either by a slight oxygen deficiency in the spinel or by the presence of a very small amount of unreacted lithium. Other results recently reported[34,35] have shown that single-phase spinels with Li/Mn ratio ~0.8 can accommodate up to 20% trivalent manganese with a corresponding deficiency in oxygen content. The unit cell parameter of "$Li_{4/3}Mn_{5/3}O_4$" preparations has also been observed to vary between 8.13 and 8.18 Å,[27,33,34] where the lower cell parameters are typically found for samples with higher total manganese oxidation state. The value $a_0 = 8.15$ Å for our sample would seem to be consistent with the relatively high Mn^{IV} content determined by chemical analysis.

Lithium extraction in acid solution results in a decrease in lattice parameter for both samples to 8.02−8.04 Å. The chemical analyses show that 89 and 98% of the original lithium content was extracted by the acid treatments of the $LiMn_2O_4$ and $Li_{4/3}Mn_{5/3}O_4$ compounds, respectively, and that proton insertion accompanies this process in $Li_{4/3}Mn_{5/3}O_4$. The bulk manganese oxidation states 3.95 and 3.97 are only slightly lower than the value of 4.0 expected for an ideal fully delithiated "λ-MnO_2" compound. After contacting in LiOH, lithium reinsertion in the λ-MnO_2 product of $LiMn_2O_4$ appears to result in >90% reconstitution of the composition of the original compound and a restoration of the unit-cell parameter of the parent material. In the case of the λ-MnO_2 product of $Li_{4/3}Mn_{5/3}O_4$, chemical analysis shows reinsertion of only 54% of the original lithium content, but the unit cell parameter is slightly *higher* in the reinserted material than for the parent compound. The bulk oxidation state determined for the reinserted material, 3.87, is nonetheless only marginally lower than that found for the parent $Li_{4/3}Mn_{5/3}O_4$, implying that lithium reinsertion has occurred mainly by reverse ion exchange with lattice protons.

Manganese K-Edge X-ray Absorption Spectra. While X-ray diffraction allows the average long-range structure of a crystalline compound to be determined and described by a unit cell, EXAFS identifies the local structure surrounding a target atom.[36] Fourier transformation of the EXAFS spectrum gives a radial distribution-like function in real space beyond the emitting atom. Figure 2 shows the relationship between the unit cell for spinel lithium manganate and the local structure around the manganese atom probed by XAS. The cubic spinel $LiMn_2O_4$[51] possesses an ideal symmetry of $Fd3m$ (O_h^7). In the crystallographic description the oxygen atoms form a cubic close packed array occupying the 32e sites of the space group, manganese atoms occupy

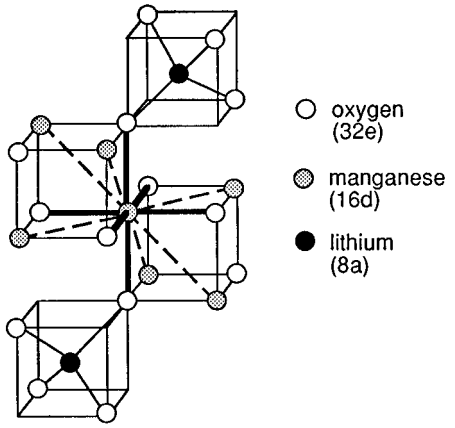

Figure 2. Part of the unit cell of $LiMn_2O_4$ showing the local structure around octahedrally coordinated manganese in an ideal spinel lattice. Mn−O bonds are represented by heavy solid lines; linear chains of manganese ions in neighboring edge-sharing octahedra are indicated by dashed lines.

the 16d sites (half of the octahedral sites), and the lithium atoms occupy the 8a sites (one-eighth of the tetrahedral sites). According to the symmetry of the system, manganese atoms are coordinated by six oxygen atoms at equal Mn−O distances (first coordination shell). A second coordination shell is formed by six equidistant manganese atoms in neighboring octahedra sharing edges with the central [MnO_6] octahedron. Neither oxygen atoms beyond the first coordination shell nor lithium atoms are expected to contribute significant signal to the EXAFS, but more distant manganese atoms arranged in coherent coordination shells may make important contributions. In addition, multiple scattering may occur, appearing in the radial distribution function as the effective sum of the different interatomic distances forming the many-legged scattering path. The amplitude of multiple scattering is enhanced when a second scattering atom lies collinearly between the emitting atom and a scatterer (the so-called "focusing" effect). Since the manganese atoms in the spinel structure form linear chains which cross perpendicularly to give the three-dimensional framework, multiple scattering of this kind may occur.

Extracting information from experimental data requires a comparison with an accurately known reference system or "standard". For this purpose, in the first section below, the spectrum of the λ-MnO_2 derived from $LiMn_2O_4$ is analyzed using ab initio functions for the backscattering amplitudes $F_i(k)$, total phase shifts $\phi_i(k)$, and photoelectron mean free path $\lambda(k)$ calculated by FEFF.[46−49] This sample contains manganese predominantly in a single oxidation state and is highly crystalline and practically free of lattice defects, allowing bond distances and coordination numbers to be compared with crystallographic values calculated for an ideal structure. In a second stage, the local structural consequences of lithium extraction and reinsertion in the $LiMn_2O_4$ and $Li_{4/3}Mn_{5/3}O_4$ systems are examined

(51) Wickham, D. G.; Croft, W. J. *J. Phys. Chem. Solids.* **1958**, *7*, 351.

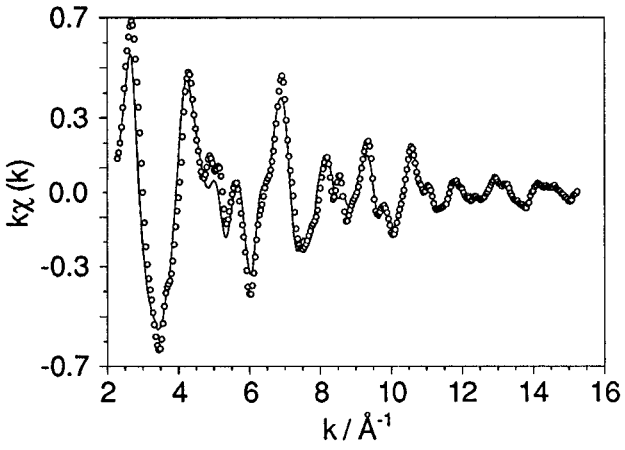

Figure 3. Experimental EXAFS data for the λ-MnO_2 product of $LiMn_2O_4$ (open circles) and the ab initio third-order multiple scattering computation for 24 coordination shells (solid line).

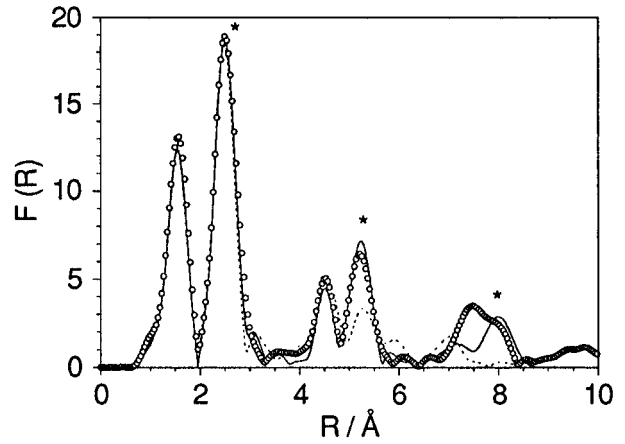

Figure 4. Fourier transformed experimental EXAFS data for the λ-MnO_2 product of $LiMn_2O_4$ (open circles), and ab initio computations for single scattering (dotted line) and multiple scattering (solid line). Peaks corresponding to scattering from the first, second, and third manganese neighbors in the linear chains are marked with asterisks. Note that in the absence of a phase correction the peaks are displaced ~0.4 Å lower than the structural values.

with reference to the EXAFS spectra. Modifications in the electronic structure and oxidation state of the manganese, determined from XANES data, are studied in the final section.

Extended X-ray Absorption Fine Structure (EXAFS). Figure 3 compares the normalized experimental EXAFS spectrum $\chi(k)$ for the λ-MnO_2 product of $LiMn_2O_4$ with simulated data computed over 24 coordination shells including multiple scattering terms up to third order (four-legged paths). This gave a better prediction of the experimental data over the whole k range than a computation using single-scattering terms only. Calculations including scattering terms higher than third order gave no further improvement, however, as most of the higher-order paths produced very weak amplitudes at the emitter and were therefore filtered out in the final calculation. Fourier transformed experimental data are compared with spectra calculated with single- and multiple-scattering paths in Figure 4. Both single- and multiple-scattering calculations satisfactorily reproduce the experimental spectrum up to ~5 Å. For R > 5 Å the multiple scattering terms have more significant effects on the data. In particular, strong contributions from multiple scattering are observed at ~5.2 and

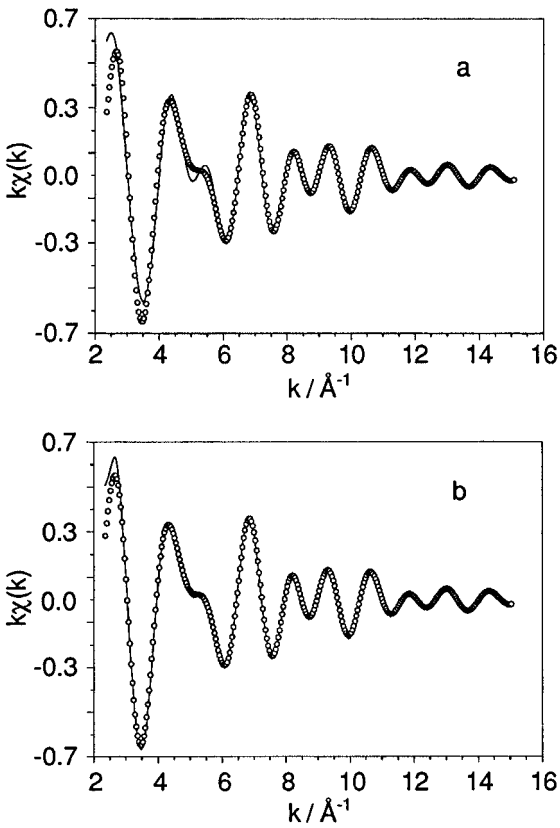

Figure 5. Experimental EXAFS data for the λ-MnO_2 product of $LiMn_2O_4$ Fourier isolated over the range 1−3 Å (open circles) and theoretical curves calculated for six oxygen and six manganese neighbours using the parameters in Table 1: (a) single scattering only; (b) including three multiple-scattering paths.

~8 Å, arising from forward scattering or "focusing" along the linear chains of edge-sharing MnO_6 octahedra to manganese atoms at respectively 2 and 3 times the distance of the nearest manganese neighbor. A peak at ~7.5 Å in the experimental data is not reproduced by the calculations but may be due to a higher order multiple-scattering path.

The comparison of the experimental and simulated data suggests that multiple scattering may be neglected for the purposes of structural refinements for the nearest oxygen and manganese neighbors. Owing to the high symmetry of the spinel structure, practically all the essential structural information can be derived by considering only the first and second coordination shells. The good agreement achieved by curve-fitting a simple single-scattering model using only two unique paths to the experimental data for the λ-MnO_2 product of $LiMn_2O_4$ Fourier isolated over the first two peaks is shown in Figure 5a. Only slight discrepancies at low k suggest that there may be a small contribution to the experimental data from multiple scattering involving first-shell oxygen atoms. Path calculations predict three such multiple-scattering paths with effective radius R_{eff} within 0.5 Å of the Fourier-isolated peaks. While their inclusion in the curve-fitting procedure improved the agreement between experimental and calculated curves, Figure 5b, it did not affect the structural parameters obtained for the Mn−O and Mn−Mn pairs. The interatomic distances, Debye−Waller factors, and energy origin corrections for the two single-scattering paths from the curve-fitting refinement are given in Table 2.

Table 2. Refined EXAFS Parameters for the λ-MnO_2 Product of $LiMn_2O_4$ Obtained Using Both Single- and Multiple-Scattering Contributions to the EXAFS up to 3 Å[a]

	R (Å)	σ (Å)	ΔE_0 (eV)	R_{cryst} (Å)
Mn−O (first coordination shell)	1.904	0.054	3.2	1.907
Mn−Mn (second coordination shell)	2.841	0.056	2.0	2.837

[a] Interatomic distances calculated using the experimental lattice parameter $a_0 = 8.02$ Å and crystallographic positions[27,50] are given for comparison.

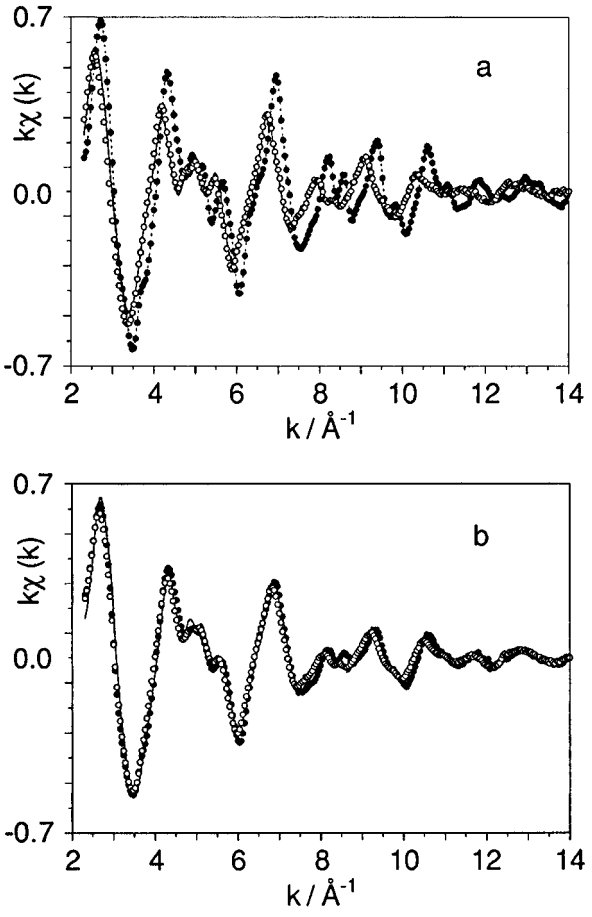

Figure 6. EXAFS spectra for (a) $LiMn_2O_4$ and (b) $Li_{4/3}Mn_{5/3}O_4$: parent compounds (solid lines), lithium-extracted samples (closed circles), and lithium-reinserted samples (open circles).

Coordination numbers were fixed at 6 for both shells in accordance with the crystallographic model.[27,50] The nearest-neighbor Mn−O and Mn−Mn distances determined for this sample using the phase shifts calculated by the FEFF code agree with crystallographic values based on the unit cell parameter to $<\pm 0.2\%$. These are slightly better than results using the tabulated phase shifts of McKale et al.[45] which gave a Mn−O distance ~1% higher than the FEFF result, although the Mn−Mn distance obtained was the same.[52]

The EXAFS spectra of the $LiMn_2O_4$ and $Li_{4/3}Mn_{5/3}O_4$ samples are compared with the spectra of their lithium-extracted products and -reinserted compounds in Figure 6. The Fourier transformed spectra, phase-shifted using the theoretical phase factor for the first Mn−O shell, are shown in Figure 7, permitting the differences between the EXAFS data to be visualised in R space.

(52) Ammundsen, B.; Burns, G. R.; Jones, D. J.; Rozière, J. *Proc. Int. Conf. Ion Exchange*; Takamatsu, Japan, 1995; pp 81−86.

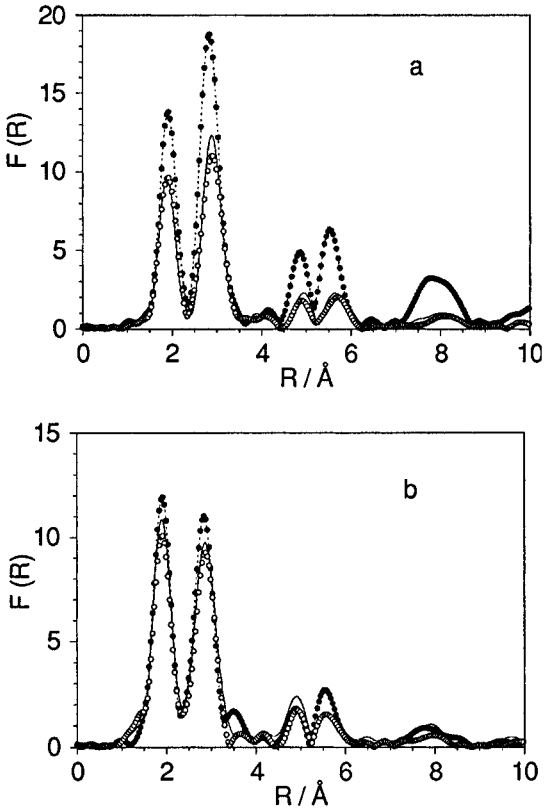

Figure 7. Fourier transformed EXAFS spectra, phase-corrected for the first Mn−O shell, for (a) $LiMn_2O_4$ and (b) $Li_{4/3}Mn_{5/3}O_4$: parent compounds (solid lines), lithium-extracted samples (closed circles), and lithium-reinserted samples (open circles).

Table 3. Structural Parameters Derived from EXAFS Analyses of Parent, and Lithium-Extracted and -Reinserted Spinels

	Mn−O		Mn−Mn		
	R (Å)	σ (Å)	R	σ (Å)	N
"$LiMn_2O_4$"	1.925	0.080	2.904	0.074	6.0
lithium-extracted	1.904	0.054	2.841	0.056	6.0
lithium-reinserted	1.926	0.074	2.903	0.082	6.1
"$Li_{4/3}Mn_{5/3}O_4$"	1.908	0.066	2.873	0.077	5.1
lithium-extracted	1.902	0.063	2.858	0.073	4.7
lithium-reinserted	1.911	0.070	2.875	0.076	5.0

The interatomic distances and Debye−Waller factors for the nearest-neighbor Mn−O and Mn−Mn pairs, determined by curve-fitting to the experimental data, are listed in Table 3. Refined values of the second-shell manganese coordination number are also given.

For both the $LiMn_2O_4$ and $Li_{4/3}Mn_{5/3}O_4$ samples, the interatomic distances refined from the EXAFS data decrease when lithium is extracted but return close to the values determined for the original compounds when lithium is reinserted. The changes in Mn−Mn distances are consistent with the variations in the unit-cell parameters calculated from the powder X-ray diffraction data, although comparison of the Mn−Mn distances from the EXAFS data with values calculated for the parent $LiMn_2O_4$ and $Li_{4/3}Mn_{5/3}O_4$ samples using the experimentally determined unit-cell parameters showed that the EXAFS values were 0.01−0.02 Å lower. The Mn−O distances determined by EXAFS showed a similar shortening. These differences are probably an effect of the lower temperature of the EXAFS experiments. Mn−O bond length variations between samples show good correlation with the average manganese

oxidation states determined by the chemical analyses. Thus the decrease in Mn−O distance when lithium is extracted from $LiMn_2O_4$ is ~0.02 Å, compared with an overall increase in manganese oxidation state from ~3.5 to 3.95. For the $Li_{4/3}Mn_{5/3}O_4$ sample the decrease in Mn−O distance resulting from lithium extraction is only ~0.006 Å, and the average oxidation state increases from 3.89 to 3.97.

It is significant that the Mn−O distance determined for the λ-MnO_2 product of $Li_{4/3}Mn_{5/3}O_4$ is slightly lower than that found for the λ-MnO_2 product of $LiMn_2O_4$, but the Mn−Mn distance is ~0.02 Å higher in the former compound. These results respectively correlate with a slightly higher average oxidation state yet higher unit-cell parameter for the former compound. The greater Mn−Mn distance in the delithiated $Li_{4/3}Mn_{5/3}O_4$ relative to the λ-MnO_2 product of $LiMn_2O_4$ may be an effect of proton insertion into the interstitial channels of the spinel lattice.

As can be clearly seen in Figure 7a, extraction of lithium from $LiMn_2O_4$ also results in a strong increase of amplitude in the overall EXAFS, which correlates with a significant decrease in the Debye−Waller factors determined for the Mn−O and Mn−Mn pairs in this sample. Reinsertion of lithium restores the EXAFS to the reduced intensity of the parent compound, with a corresponding return of the Debye−Waller factors close to their original values. These strong changes, which are not observed in the case of $Li_{4/3}Mn_{5/3}O_4$, suggest that extraction of lithium from $LiMn_2O_4$ results in a more ordered local arrangement, but that this order is lost when lithium is reinserted into the λ-MnO_2 compound.

The origin of the changes in local structural order detected by EXAFS between $LiMn_2O_4$ in its lithiated and delithiated forms can be found in the change in average manganese oxidation state between ~3.5 and ~4. An average manganese valence of 3.5 is a critical limit below which local distortions around Jahn−Teller Mn^{III} ions in octahedral sites of the spinel lattice can no longer be supressed by the presence of non-Jahn−Teller Mn^{IV} ions. At this critical valence, $LiMn_2O_4$ contains small localized regions in which several Mn^{III} ions occupy adjacent octahedral positions and cooperative tetragonal distortion of the octahedra overcomes the strains imposed by the surrounding cubic lattice.[51] Due to the localized nature of the distortion and the random orientation of small tetragonal domains along all three cubic axes with respect to the bulk structure, the effects are difficult to detect by diffraction against the overall cubic symmetry of the long-range structure. However, a recent report has shown that microdomains of tetragonal phase in $LiMn_2O_4$ can be resolved by powder X-ray diffraction below 280 K.[53] EXAFS is very sensitive to local structural distortions, and the disordering effects of different manganese symmetries in the same compound are clearly observed in the spectra here, recorded at 77 K. It is striking that the local structural distortion which is alleviated by the oxidative extraction of lithium is easily reestablished by the reverse process.

In contrast, the Debye−Waller factors determined for the $Li_{4/3}Mn_{5/3}O_4$ sample show little change on lithium extraction or reinsertion. The number of manganese

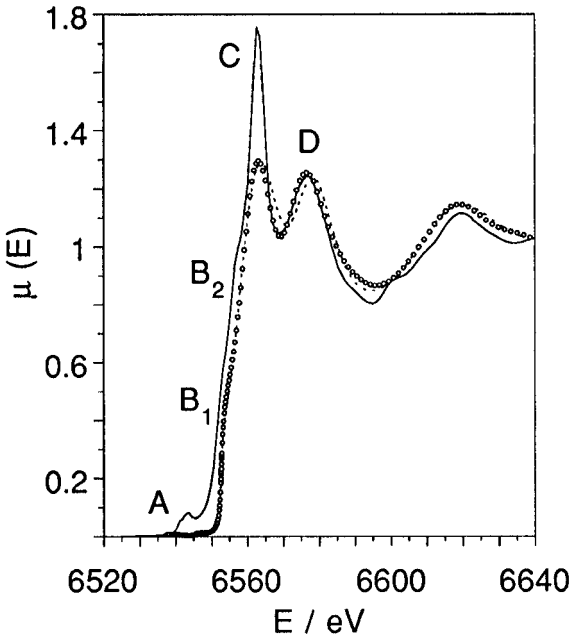

Figure 8. Experimental X-ray absorption edge spectrum of the λ-MnO_2 product of $LiMn_2O_4$ (solid line), and ab initio third-order multiple-scattering simulations over 24 (open circles) and four (dotted line) coordination shells. XANES features A−D in the experimental spectrum are described in the text. Simulated spectra have been displaced +11 eV for comparison with the experimental data.

in the second coordination shell for these samples was refined between 4.7 and 5.1, which agrees with the crystallographic model[27] in which approximately one-sixth of the 16d octahedral sites are substituted by lithium ions, giving rise to octahedral vacancies in the lithium-extracted material. Small but significant displacements of both manganese and oxygen atoms from their average crystallographic positions are therefore expected for these materials, including local perturbations due to inserted protons bonded to oxygen atoms.[17] The Debye−Waller factors for both the lithium-containing and the delithiated $Li_{4/3}Mn_{5/3}O_4$ samples are consequently higher than those observed for the highly ordered λ-MnO_2 product of $LiMn_2O_4$.

X-ray Absorption Near-Edge Structure (XANES). The XANES spectra of the spinel manganese oxide samples were characterized in each case by the features labeled A to D shown for the experimental spectrum of the λ-MnO_2 product of $LiMn_2O_4$ in Figure 8. Pre-edge features A result from transitions to bound final states in 3d orbitals and appear in the K-edge XANES of most 3d elements. The main absorption edge rises in two distinct steps which may be distinguished as two inflection points B_1 and B_2. Two strong resonances C and D are present just above threshold, beyond which the spectra show the fine structure of weaker intensity characterized as the EXAFS.

XANES resonances are typically distinguished from the EXAFS regime by stronger multiple scattering character. At the low energies just above the absorption edge the mean free path of the photoelectron can be quite large and there is a high probability of off-linear scattering involving several atoms. As shown in Figure 8, ab initio simulation of the $\mu(E)$ spectrum of λ-MnO_2 over 24 coordination shells, including multiple scattering up to third order and paths up to 18 Å, predicts two strong resonances at relative energies corresponding to

(53) Yamada, A.; Tanaka, M. *Mater. Res. Bull.* **1995**, *30*, 715.

the experimental features C and D (the simulated spectrum has been displaced 11 eV to higher energy as the absolute energy scale, based on atomic calculations, results in a threshold energy slightly lower than that experimentally observed for the manganese dioxide system). Reducing the multiple scattering calculation to only four shells gave a very similar result to the 24-shell model, but a calculation for only two shells resulted in a single broad resonance. It can be concluded that the inclusion of single and multiple scattering to the third and fourth coordination shells, consisting of oxygen atoms at distances 3.3−3.5 Å from the central manganese atom, is therefore essential to predict two well-defined scattering resonances. However, the strong experimental intensity of the resonance C was not reproduced by the calculations, although the simulated intensity and line width of the resonance D are in good agreement with experiment. The double inflection in the rising edge is also absent from the theoretical simulation. These discrepancies between the theoretical model and the experimental data may derive from electronic effects in the threshold region which could not be predicted by the self-energy model[49] for the photoelectron used in the calculation.

Figure 9 compares the X-ray absorption edge spectra of $LiMn_2O_4$ and $Li_{4/3}Mn_{5/3}O_4$ with the spectra of their lithium-extracted and -reinserted products. The spectra of α-Mn_2O_3 and β-MnO_2 are also shown. The energy positions of the structures A−D (see Figure 8) are tabulated in Table 4 for each of the spinel samples. The positions of the pre-edge peaks *A* and the strong resonances C and D are those of the maxima in the absorption spectra, determined from the zero nodes of the first derivative curves also shown in Figure 9. The energies of the fine structures B in the absorption edges are taken as the inflection points, determined from the maxima in the first-derivative curves.

Differences in the electronic state of the absorbing manganese atom in the samples are shown by the variations in the position of the absorption edge in the spectra, which correlate closely with the average effective charge on the manganese.[37−40] In the molecular orbital model, the K-absorption edge in manganese oxides is determined by the threshold of dipole allowed transitions to p-like antibonding states of the MnO_6 octahedron. The greater overlap of Mn and O orbitals when the manganese is in a more oxidized state results in an increase of the energies of these outer molecular levels relative to those of the core levels, giving rise to a higher threshold absorption energy. The difference is clearly observed in the spectra of α-Mn_2O_3 and β-MnO_2 where the absorption edge of β-MnO_2 is found approximately 3.5 eV higher in energy than that of α-Mn_2O_3. The spectra of the spinel compounds differ from the spectra of α-Mn_2O_3 and β-MnO_2 in that two distinct inflection points B_1 and B_2 appear in the absorption edges of the spinel compounds. However, the overall position of the absorption edge of the $LiMn_2O_4$ sample is approximately half-way between those of α-Mn_2O_3 and β-MnO_2, whereas that of the $Li_{4/3}Mn_{5/3}O_4$ sample is displaced 1.5 eV to higher energy relative to the $LiMn_2O_4$ sample, and therefore lies close to the absorption edge of β-MnO_2. These observations are in good agreement with the higher bulk oxidation state and shorter Mn−O bond distance determined for the $Li_{4/3}Mn_{5/3}O_4$ compound relative to $LiMn_2O_4$.

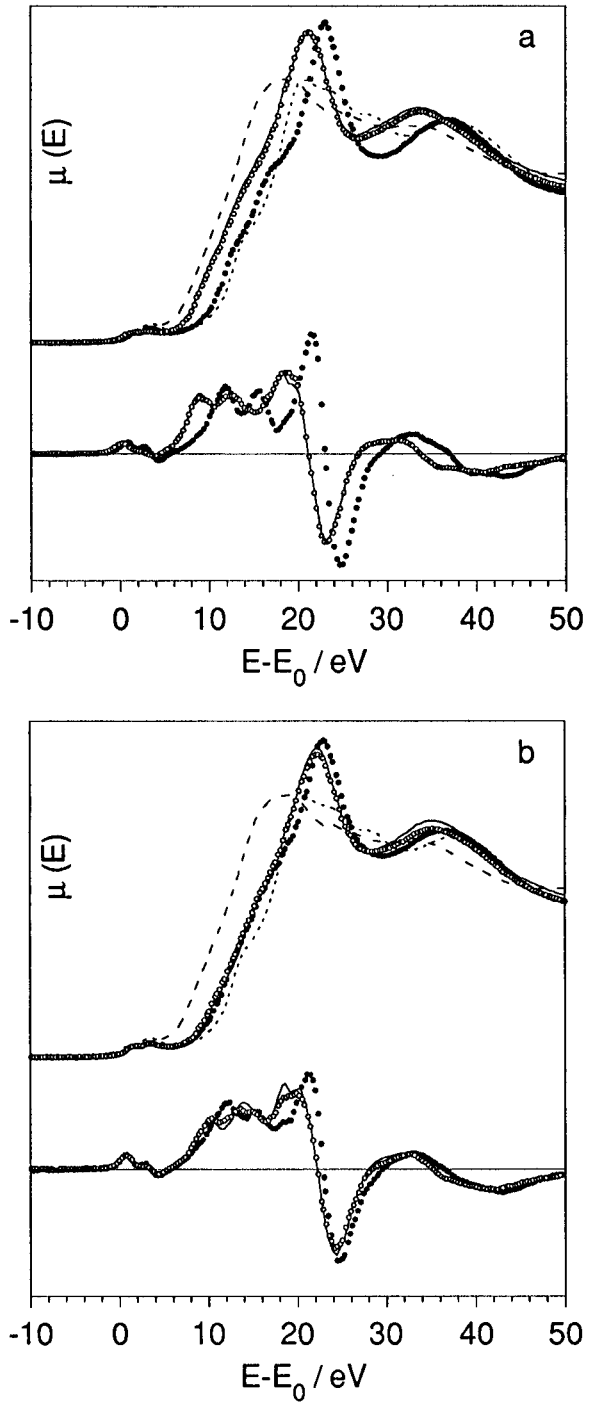

Figure 9. XANES spectra (above) and first derivative curves (below) for (a) $LiMn_2O_4$ and (b) $Li_{4/3}Mn_{5/3}O_4$: parent compounds (solid lines), lithium-extracted samples (closed circles), and lithium-reinserted samples (open circles). Spectra of α-Mn_2O_3 (long dashes) and β-MnO_2 (short dashes) are also shown.

Table 4. XANES Energy Positions $E - E_0$ (eV) for the Parent and Lithium-Extracted and -Reinserted Spinel Compounds

sample	A_1	A_2	B_1	B_2	C	D
"$LiMn_2O_4$"	1.4	2.9	8.9	12.4	21.2	33.6
lithium-extracted	1.7	3.5	11.9	15.4	23.0	37.0
lithium-reinserted	1.4	2.9	9.1	12.4	21.2	33.7
"$Li_{4/3}Mn_{5/3}O_4$"	1.7	3.5	10.4	13.9	22.2	35.2
lithium-extracted	1.7	3.5	12.1	15.2	22.9	36.6
lithium-reinserted	1.7	3.5	10.4	13.9	22.2	35.2

Extraction of lithium from $LiMn_2O_4$ results in an overall shift of the absorption spectrum so that the edge

of the delithiated "λ-MnO_2" sample nearly superimposes on that of β-MnO_2. A change in the structure of the pre-edge peaks A is observed, and narrowing of the resonances C and D. The main edge structures B_1 and B_2 are also strongly affected by the lithium extraction from $LiMn_2O_4$, changing from relatively broad features to sharply defined shoulders with an overall displacement of the inflection points by ~3 eV to higher energy. Reinsertion of lithium results in almost complete restoration of the spectrum of the parent compound, including the position of the edge and rebroadening of the main edge structure and resonances C and D. The shifts in the absorption edge observed for the $LiMn_2O_4$ sample agree well with the chemical analyses of manganese oxidation state and the changes in Mn−O distance determined by EXAFS which show oxidation and reduction of manganese to be the dominant mechanism of lithium extraction and reinsertion for this compound. The sharpening and rebroadening of the XANES features recalls the effects of local structural order seen in the EXAFS spectra of these samples.

Supporting information specific to the valence electronic structure at the manganese centres can be obtained from the pre-edge structure A, which arises from transitions to final d-like states fully localised within the first coordination shell. Although the 1s → 3d transition is generally weak in octahedral coordination because it is formally dipole forbidden, these states show up in absorption due to direct quadrupole coupling to the electromagnetic radiation or to the mixing of 3d and 4p orbitals in the local structure.[42,54] The pre-edge structures of $LiMn_2O_4$ and its lithium-extracted and -reinserted products are compared with the pre-edge spectra of α-Mn_2O_3 and β-MnO_2 in Figure 10a, after subtraction of the interpolated tail of the main edge from the spectra of Figure 9. The pre-edge spectra of the parent $LiMn_2O_4$ compound and the lithium-reinserted sample are very similar to each other with two maxima at identical energies for the two samples. The positions of these peaks are consistent with a manganese valency intermediate between those of α-Mn_2O_3 and β-MnO_2. After extraction of lithium from $LiMn_2O_4$ both a chemical shift to higher energy and a change in the structure of the peaks is observed, so that the two bound states resolved in the spectrum of the lithium-extracted "λ-MnO_2" sample are observed at the same energies as in the spectrum of β-MnO_2. A doublet of two overlapping peaks at these energies in the pre-edge spectrum appears to be characteristic of manganese(IV) oxides, and only the intensity is observed to vary for different structural modifications.[42]

In the case of the $Li_{4/3}Mn_{5/3}O_4$ sample, the overall chemical shift of the main absorption edge to higher energy after lithium extraction is less than 0.4 eV. Only the inflection points B_1 and B_2 appear to show a greater displacement due to a modification in the shapes of the corresponding structures. The resonances C and D also show small shifts to higher energy but little change in shape or intensity. Reinsertion of lithium in the λ-MnO_2 product of $Li_{4/3}Mn_{5/3}O_4$ again led to almost complete restoration of the spectrum of the parent compound. The very small edge shifts relative to the $LiMn_2O_4$ compound support an ion-exchange mechanism as the dominant

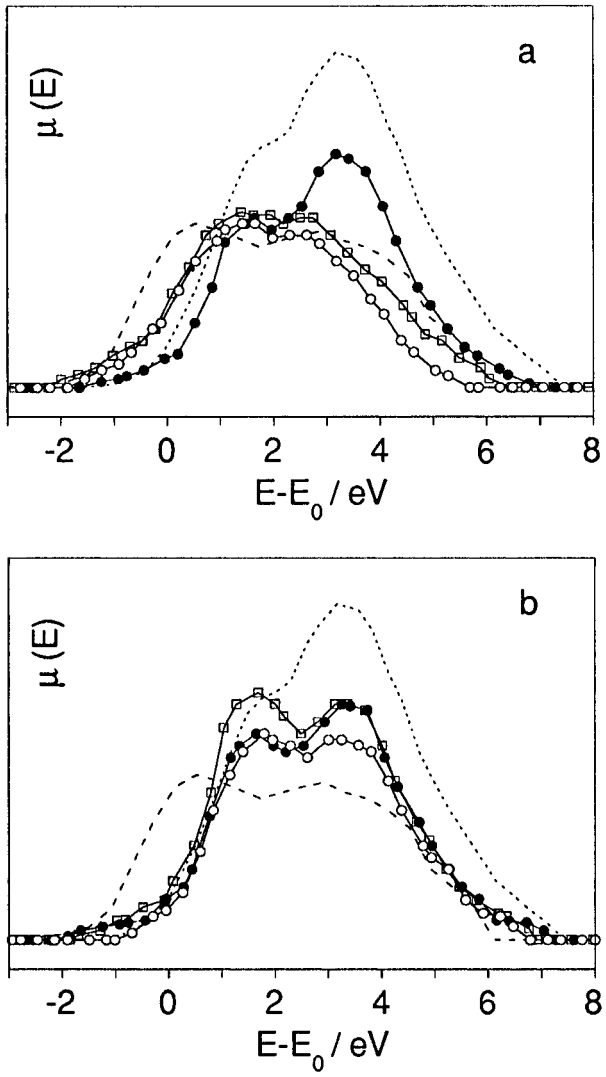

Figure 10. Background-corrected pre-edge spectra for (a) $LiMn_2O_4$ and (b) $Li_{4/3}Mn_{5/3}O_4$: parent compounds (open squares), lithium-extracted samples (closed circles), and lithium-reinserted samples (open circles), compared with spectra for α-Mn_2O_3 (long dashes) and β-MnO_2 (short dashes).

extraction and reinsertion mechanism for the $Li_{4/3}Mn_{5/3}O_4$ sample, with only a small contribution from a redox process. Furthermore lithium extraction from this sample results in practically no modification of the pre-edge peaks. Figure 10b compares the pre-edge spectrum of the $Li_{4/3}Mn_{5/3}O_4$ sample with its lithium-extracted and -reinserted products. The peaks for the parent $Li_{4/3}Mn_{5/3}O_4$ compound correlate with those of β-MnO_2 and undergo no displacement in energy when lithium is extracted or reinserted, consistent with a manganese valency close to 4 in all three samples. The pre-edge data therefore fully support the model of a dominant ion-exchange mechanism for $Li_{4/3}Mn_{5/3}O_4$ entailing only trivial changes in the local electronic structure of the manganese.

We note that previous assignments of the double inflection in the absorption edge of spinel manganese oxides to two different manganese sites and/or two different manganese oxidation states[39,41] are unsupported by the data presented here. The EXAFS data are in agreement with the crystallographic models of a single manganese site in the samples, and the presence of two inflection points is observed for both the λ-MnO_2 samples and the lithiated spinels and is therefore

(54) Grunes, L. A. *Phys. Rev. B* **1983**, *27*, 2111.

apparently independent of oxidation state. Furthermore the displacements of B_1 and B_2 with lithium extraction and reinsertion in the spectra of both the $LiMn_2O_4$ and $Li_{4/3}Mn_{5/3}O_4$ samples are of approximately the same magnitude and follow the shift of the resonance D in both cases. The definition of the double inflection may also be correlated with the relative degree of long-range order in the samples seen in the EXAFS. These observations strongly support a structural rather than chemical origin for the XANES features B.

Conclusions

Changes in Mn−O bond distances determined from EXAFS and the evolutions of the XANES spectra of $LiMn_2O_4$ and $Li_{4/3}Mn_{5/3}O_4$ support chemical analyses which show different degrees of oxidation−reduction in these compounds when lithium is extracted and reinserted. For $LiMn_2O_4$ the X-ray absorption data are consistent with a predominantly redox mechanism in which lithium extraction from a mixed Mn^{III}/Mn^{IV} compound gives a Mn^{IV} product with higher local structural order than the parent material. The reaction has been described by Hunter[1] and by Ooi and coworkers:[7−9,12]

$$4LiMn^{III}Mn^{IV}O_4 + 8H^+ \rightarrow 3Mn^{IV}{}_2O_4 + 4Li^+ + 2Mn^{2+} + 4H_2O$$

Reinsertion of lithium in the λ-MnO_2 product occurs with reduction of an equivalent of lattice Mn^{IV} to Mn^{III}, resulting in almost complete reconstitution of the structure and composition of the original material, in agreement with the reaction proposed by Ooi et al.:[7−9]

$$Mn^{IV}{}_2O_4 + n\mathrm{LiOH} \rightarrow Li_nMn^{III}{}_nMn^{IV}{}_{2-n}O_4 + n/2H_2O + n/4O_2$$

In contrast, the XAS data clearly demonstrate that lithium extraction from $Li_{4/3}Mn_{5/3}O_4$ results in trivial changes in local electronic structure and only a small decrease in interatomic distances. The data are consistent with lithium−proton exchange being the dominant extraction mechanism for this material. The resulting "λ-MnO_2" is therefore chemically distinct from the delithiated product of $LiMn_2O_4$ in protonic lattice species, which may be present as both hydroxyl and water groups.[17] Although XAS shows that ∼50% relithiation is sufficient to reestablish the essential local structure of the parent compound, the partially relithiated product must remain high in proton content. Investigations of the chemical and physical processes which occur during proton−lithium exchange are currently being undertaken within our group and will be the subject of future reports.

Acknowledgment. The authors thank the CEA-CNRS-MENESR for access to the facilities at LURE and Françoise Villain (LURE) for her assistance. Financial support from the French Ministère des Affaires Etrangères through the France-New Zealand Cultural Exchange is acknowledged. B.A. also acknowledges grants from the Royal Society of New Zealand and the Internal Grants Committee of Victoria University of Wellington.

CM960287S